

## COBALT LOADING EFFECTS ON THE PERFORMANCE AND STABILITY OF GRAPHENE NANOSHEETS SUPPORTED COBALT CATALYST IN FISCHER-TROPSCH SYNTHESIS

Fateme Hasanpour<sup>1</sup>, Saba Karimi<sup>1</sup>, Sanaz Anahid<sup>2</sup>, Ahmad Tavasoli<sup>1</sup>, Yahya Zamani<sup>2</sup>

<sup>1</sup> School of Chemistry, College of Science, University of Tehran, Tehran, Iran

<sup>2</sup> Gas Division, Research Institute of Petroleum Industry, Tehran, Iran

Received August 22, 2015; Accepted November 30, 2016

---

### Abstract

The effects of cobalt loading on the performance of graphene nanosheets (GNS) supported cobalt catalysts in Fischer-Tropsch synthesis (FTS) are investigated. Up to 40 wt. % cobalt is added to the support by the impregnation method. The physico-chemical properties of the catalysts are investigated by TPR, TPD, BET, XRD, TEM and H<sub>2</sub> chemisorption methods. The performance of the catalysts was assessed in a fixed bed micro-reactor at 220°C, 18 bars and H<sub>2</sub>/CO ratio of 2. The results were compared with those of Co/γ-alumina. Using GNS as cobalt catalyst support decreased the average cobalt particles size from 16 to 6 nm, increased cobalt dispersion from 6 to 21% and improved the catalyst reducibility by a factor of 2.25. The performance of catalyst in FTS enhanced by a factor of 1.8 in comparison with that obtained for Co/γ-Al<sub>2</sub>O<sub>3</sub>. The products selectivity showed a slight shift to lower molecular weight hydrocarbons. For Co/GNS catalysts the FTS rate increased with increasing the amount of cobalt loading reached a maximum at the cobalt loading of 30 wt.% and then slightly decreased. However for Co/γ-Al<sub>2</sub>O<sub>3</sub> catalysts the maximum activity is obtained at 25wt.% cobalt loading. Using GNS as catalyst support increased the catalyst lifetime.

**Keywords:** Fischer-Tropsch synthesis; Graphene nanosheets; Cobalt Loading; performance; Stability.

---

## 1. Introduction

Fischer-Tropsch synthesis produces hydrocarbons from syngas, which is a mixture of carbon monoxide and hydrogen. Depending on catalyst, reactor type and reaction conditions, FT synthesis could produce a wide range of hydrocarbons such as light hydrocarbons, gasoline, diesel fuel and wax [1]. One important focus in development of this process is improving the catalyst activity by increasing the number of surface active Co sites which are stable under the reaction conditions [2]. Previous studies showed that a drawback of the FTS commercial catalysts (cobalt dispersed on porous carriers such as SiO<sub>2</sub>, Al<sub>2</sub>O<sub>3</sub> and TiO<sub>2</sub>) is their support reactivity toward cobalt, which during preparation or catalysis results in the formation of mixed compounds that are reducible only at very high reduction temperatures [3-4]. Formation of these compounds depends on the nature of support and interactions of support with cobalt. Furthermore, interactions of cobalt with support may also depend on the amount of metal loading [5].

In recent years, some novel carbon materials, such as carbon nanofibers (CNFs), carbon nanotubes (CNTs) and graphene nanosheets (GNS) have become the most interesting catalyst supports [6]. CNFs and CNTs have been used as cobalt FTS catalyst supports. Compared to CNFs and CNTs, GNS has better structural, mechanical and chemical stability and improved electronic properties [7]. GNS with its two-dimensional sheet of sp<sup>2</sup>-hybridized carbon, provides a high specific surface area and influences the dispersion of the metal clusters and also electronically modifies the active metal sites [7].

In this work, the catalytic properties of Co/GNS catalyst prepared by the sequential aqueous incipient wetness impregnation method are presented. The cobalt loading was varied from 5 to 35 wt.%. The physico-chemical characteristics and catalytic performance of the catalysts are

evaluated and the results are compared by commercial  $\gamma$ -alumina supported cobalt catalyst with the same cobalt loading.

## **2. Experimental**

### **2.1. Catalyst preparation**

RIPI-GNS (purity > 99.5%) was used as support material for preparation of cobalt catalysts. GNS supported catalysts (C<sub>1</sub>-C<sub>7</sub>) were prepared with cobalt loadings of 5, 10, 15, 20, 25, 30 and 35wt.%. Prior to catalyst preparation, support was refluxed with 30% HNO<sub>3</sub> at 120°C overnight, washed with distilled water several times and dried at 120°C for 6 h. This approach creates oxygen containing OH functional groups on both the edges and basal plane of GNS, which can be used as chemically active anchoring sites for metal particles. The catalysts were prepared using an aqueous solution of cobalt nitrate. The sequential impregnation method was used to add Co(NO<sub>3</sub>)<sub>2</sub>·6H<sub>2</sub>O (99.0%, Merck) to the supports. After impregnation, catalysts were dried at 120°C and then were calcined at 350°C for 4 h with a heating rate of 1°C/min. Also one  $\gamma$ -alumina supported (Condea Vista Catalox B  $\gamma$ -alumina) catalyst (A<sub>1</sub>) with cobalt loading of 15 wt.% was prepared just for comparison purposes. This catalyst was dried at 120°C and calcined at 350°C for 3 h with a heating rate of 1°C/min. The catalysts nomenclature and compositions are listed in Table 1.

### **2.2. Catalyst characterization**

#### **2.2.1. Inductively coupled plasma**

Weight percentages of Co metal in the catalysts were measured by inductively coupled plasma (ICP) method using a Varian VISTA-MPX instrument.

#### **2.2.2. Transmission electron microscopy (TEM)**

Catalysts were suspended in methanol using an ultrasonic bath and dropped onto a carbon coated copper grid to take the TEM images of the samples using a Philips CM20 (100 kV) transmission electron microscope equipped with a NARON energy-dispersive spectrometer with a germanium detector.

#### **2.2.3. BET surface area measurements/BJH pore size distributions**

BET surface area measurements were carried out using an ASAP-2010 system from Micromeritics. In each trial, a weight of approximately 0.25 g of sample was degassed at 200°C for 4h under 50 mTorr vacuum and the BET area, pore volume, and average pore radius were determined.

#### **2.2.4. X-ray diffraction**

A Philips analytical X-ray diffractometer (XPertMPD) with monochromatized Cu/K $\alpha$  was used to record the X-ray diffraction patterns (XRD) of the catalysts. Co<sub>3</sub>O<sub>4</sub> crystallite size was estimated based on the Debye-Scherrer equation.

#### **2.2.5. Temperature programmed reduction (TPR)**

H<sub>2</sub>-TPR was conducted on catalysts using Micromeritics TPD-TPR 2900 system equipped with a thermal conductivity detector (TCD). First traces of water and gases were removed from the catalysts by purging with helium at 140°C. Then, after cooling to 40°C, TPR of each sample was performed using 5% H<sub>2</sub> in Ar stream with flow rate of 40 ml/min at atmospheric pressure at a linearly programmed heating (10°C/min) up to 850°C.

#### **2.2.6. Hydrogen chemisorption and reoxidation**

The amounts of chemisorbed hydrogen on the catalysts were measured using the Micromeritics TPD-TPR 290 system. 0.25 g of the calcined catalyst was reduced under hydrogen at 400°C for 20 h and then cooled to 50°C under hydrogen. Then the flow of hydrogen was switched to argon at the same temperature, which lasted for about 30 min in order to remove the physi-

cally sorbed hydrogen. Afterwards, the temperature programmed desorption (TPD) of the samples was obtained by increasing the temperature of the samples, with a ramp rate of 20°C/min, to 400°C under the argon flow. After TPD of hydrogen, the sample was reoxidized at 400°C by pulses of 10% oxygen in helium to determine the extent of reduction. It is to note that during reoxidation of the catalysts, no CO<sub>2</sub> peak is observed indicating that GNS has not reacted with oxygen. The data were used to determine the cobalt dispersion, percentage reduction and cobalt average crystallite size. The dispersion, percentage reduction and particle diameter are calculated by the following formula [8].

$$\%Dispersion = \frac{\text{number of Co}^0\text{atoms on surface}}{\text{number of Co atoms in sample}} \times 100 \quad (1)$$

$$\text{Fraction reduced} = \frac{O_2 \text{ Uptake} \times \frac{2}{3} \times \text{atomic weight}}{\text{Percentage metal}} \quad (2)$$

$$\text{Diameter (nm)} = \frac{6000}{\text{Density} \times \text{maximum area} \times \text{dispersion}} \quad (3)$$

### 2.3. Reaction setup and experimental outline

The catalysts were evaluated in terms of their Fischer–Tropsch synthesis (FTS) activity (g HC produced/g cat/min) and selectivity (the percentage of the converted CO that appears as a hydrocarbon product) in a tubular fixed-bed micro-reactor. Typically, 0.6 g of the catalyst diluted with 2 g of SiC to eliminate the temperature gradient and charged into the reactor. The reactor temperature was maintained constant ( $\pm 1^\circ\text{C}$ ) by a PID temperature controller. Brooks 5850 mass flow controllers were used to add H<sub>2</sub> and CO at the desired flow rates and the mixed gases entered through the top of the reactor. The catalysts were reduced in H<sub>2</sub> flow at 400°C, with a heating rate of 1°C/min for 16 hours. Following activation, syngas (H<sub>2</sub>/CO = 2) was injected with a flow rate of 45 ml/min. The temperature and pressure were maintained at 220°C and 1.8 MPa, respectively. Products were continuously removed from the vapor and passed through two traps, one maintained at 100°C (hot trap) and the other at 0°C (cold trap). The uncondensed vapor stream was reduced to atmospheric pressure through a pressure letdown valve. The outlet flow was measured with a bubble-meter and its composition quantified using an on-line GC. The contents of hot and cold traps were removed every 24 h, the hydrocarbon and water fractions were separated, and then analyzed by a Varian 3800 gas chromatograph equipped with a capillary column and a flame ionization detector.

## 3. Results and discussion

### 3.1. Supports and catalysts characterization

Results of surface area measurement and textural properties of the supports and catalysts are listed in Table 1.

Table 1. BET surface area and XRD results

Support/Catalyst	Co (wt.%)	BET (m <sup>2</sup> /g)	Pore volume (single point) (cm <sup>3</sup> /g)	Average pore radius (nm)	d <sub>Co304</sub> (nm) determined by XRD
$\gamma$ -Al <sub>2</sub> O <sub>3</sub>	-	270	0.639	4.72	-
GNS	-	495	2.11	9.94	-
5Co/GNS5(C <sub>1</sub> )	4.85	459	0.951	8.28	6.6
10Co/GNS5(C <sub>2</sub> )	10	392	0.765	8.28	7.1
155Co/GNS5(C <sub>3</sub> )	14.88	368.7	0.66	7.18	7.8
20Co/GNS5(C <sub>4</sub> )	19.9	297.2	0.44	6.41	8.8
25Co/GNS5(C <sub>5</sub> )	24.87	260.7	0.42	6.39	9.8
30Co/GNS5(C <sub>6</sub> )	19.91	231.1	0.37	6.36	11.4
35Co/GNS5(C <sub>7</sub> )	34.86	20735	0.37	6.06	13.2
15Co/ $\gamma$ -Al <sub>2</sub> O <sub>3</sub> (A <sub>1</sub> )	14.84	214	0.439	4.26	14.7

GNS presents an ideal two-dimensional material composed of layers of atoms organized in a hexagonal lattice and connected by  $sp^2$  in-plane carbon-carbon bonds. This structure exhibits a high specific surface area [9]. As shown, in the case of GNS supported catalysts, by increasing the metal content, surface area decreases and pore blocking increases. Blockage of the smaller pores in the case of the catalysts with higher cobalt loading will result higher values of the average pore size in comparison to the other catalysts. As shown, the decrease of BET surface area and pore volume is higher in the case of the catalysts supported on GNS. Loading of 15wt.% cobalt on  $\gamma$ - $Al_2O_3$  decreased the BET surface area from 270 to 214  $m^2/g$  (indicating 20.7% decrease), However the same loading of cobalt on GNS, decreased the BET surface area for 495 to 368.7  $m^2/g$  (indicating 25.5% decrease).

Figure 1a shows the TEM image of the 15wt.% Co/Graphene( $C_3$ ) catalyst after calcination, at 350°C. The dark spots represent the cobalt oxides which are attached to the support surface. The TEM image shows remarkably uniform cobalt nanoparticles that are well dispersed on the graphene surface. As shown, the well-dispersed metal nanoparticles with an average size of 3-7 nm are formed. Figure 1b shows the TEM image of the 15wt.% Co/ $\gamma$ - $Al_2O_3$  ( $A_1$ ) catalyst after calcination at 350°C. The TEM micrograph of the calcined 15wt.% Co/ $\gamma$ - $Al_2O_3$  catalyst reveals that the catalyst particles are dispersed on the surface of alumina. Dark spots represent the cobalt oxides which are attached to the surface of alumina. The cobalt oxide particles inside the pores of alumina are moderately uniform and the most abundant ones have sizes in the range of 5-15 nm.

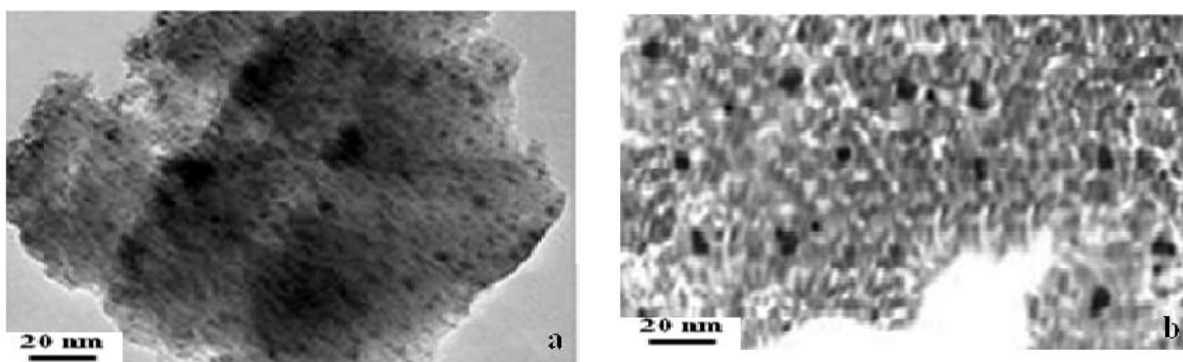


Figure 1. TEM images of the 15wt.% Co/Graphene ( $C_3$ ) and 15wt.% Co/ $\gamma$ - $Al_2O_3$  ( $A_1$ )

XRD patterns of the catalysts are shown in Figure 2. In the XRD of  $A_1$  catalyst peaks at 46.1 and 66.5° correspond to  $Al_2O_3$ , while the other peaks, except that at 49° peak, which is attributed to the cobalt aluminates [10-11], relate to the different crystal planes of  $Co_3O_4$ . In the patterns of GNS supported catalysts, the peaks at 25 and 43° correspond to GNS [12]. The other peaks with  $2\theta$  values of 31.3, 36.8, 45.8, 59.4, and 65.3 could be attributed to the  $Co_3O_4$  spinel phase in the catalysts [13]. The XRD patterns of low loaded Co/GNS catalysts show two broad peaks ( $2\theta$  values of 25° and 43°) due to amorphous GNS and by increasing the cobalt loading there are more Co particles on GNS surface which might be able to occupy more anchoring sites (defects) and consequently creates less amorphous structures [14]. In contrast to the 49° peak in the spectrum of  $A_1$  catalyst, which is attributed to the cobalt aluminates, in the XRD patterns of GNS supported catalysts no peak was observed indicating formation of cobalt support compounds. The peak at 36.8° is the most intense peak of  $Co_3O_4$  in XRD pattern of all catalysts [13]. Table 1 shows the average  $Co_3O_4$  crystallite sizes calculated from XRD spectrum and Scherrer equation at  $2\theta$  value of 36.8°. The results show that by increasing the cobalt loading, the average cobalt crystallite size increases. Agglomeration of cobalt particles is the main reason of increasing the average crystallite sizes. Comparing the average  $Co_3O_4$  crystallite size for 15wt.% Co/GNS and 15wt.% Co/ $\gamma$ - $Al_2O_3$  catalysts, reveals that the average  $Co_3O_4$  crystallite size for GNS supported catalyst is smaller than that of  $\gamma$ -

Al<sub>2</sub>O<sub>3</sub>supported catalyst. Higher surface area of GNS support will lead to better distribution of particles, which in turn leads to lower cobalt cluster sizes [12].

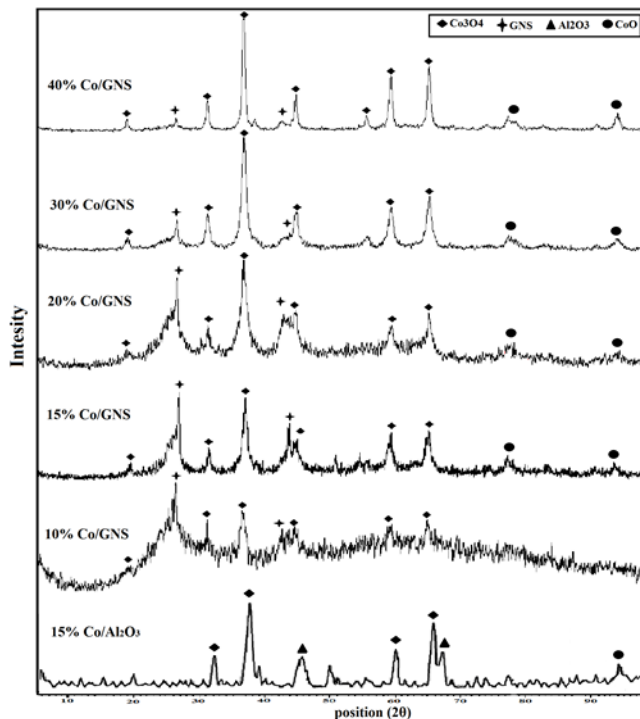


Figure 2. XRD patterns of the calcined Co/GNS and Co/Al<sub>2</sub>O<sub>3</sub> catalysts

The TPR spectra of the calcined catalysts are shown in Figure 3.

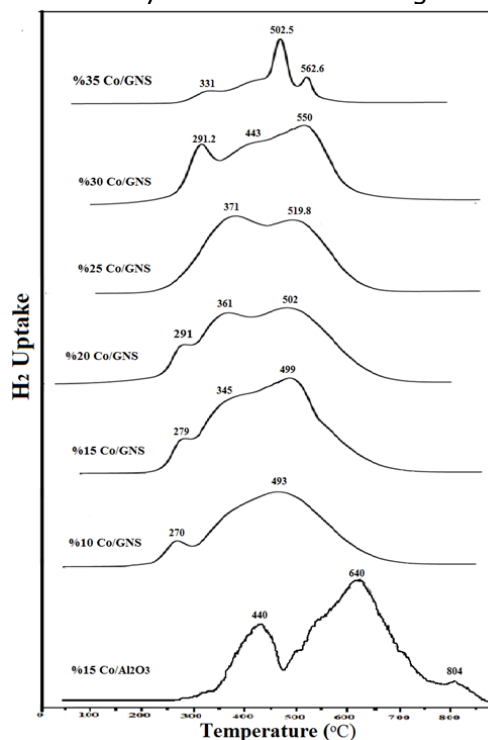


Figure 3. TPR patterns of the calcined Co/GNS and Co/Al<sub>2</sub>O<sub>3</sub> catalysts from 40 to 850°C

In this Figure 3, in the TPR profile of alumina supported catalyst the first peak is typically assigned to the reduction of  $\text{Co}_3\text{O}_4$  to  $\text{CoO}$ , although a fraction of the peak likely comprises the reduction of the larger, bulk-like  $\text{CoO}$  species to  $\text{Co}^0$ . The second peak, with a broad shoulder is mainly assigned to the second step reduction, which is mainly reduction of  $\text{CoO}$  to  $\text{Co}^0$ . This peak also includes the reduction of cobalt species that interact with the support, which extends the TPR spectra to higher temperatures [15]. As shown in this Figure, interaction between the cobalt and alumina support shifts the reduction of some cobalt species to temperatures about  $750^\circ\text{C}$ . Also a reduction feature for  $\text{A}_1$  catalyst observed in the temperature range of  $700\text{--}950^\circ\text{C}$ , with a maximum centered at about  $804^\circ\text{C}$ . Such a high reduction temperature might be assigned to the reduction of cobalt aluminates species formed by reaction of highly dispersed  $\text{CoO}$  with the alumina. In fact, cobalt aluminates were shown to reduce at temperatures well above  $800^\circ\text{C}$ , while bulk  $\text{Co}_3\text{O}_4$  became completely reduced at temperatures below  $500^\circ\text{C}$  [11, 15]. All these features suggest that part of the cobalt in the alumina supported cobalt catalysts strongly interacts with the support, as also evidenced from XRD patterns. Figure 3 also shows the TPR of the GNS supported cobalt catalysts. In the case of  $\text{Co}/\text{GNS}$  samples, the first and second reduction peaks were found at the ranges of  $271\text{--}310^\circ\text{C}$  and  $515\text{--}540^\circ\text{C}$  [16]. As shown, the first and second reduction peaks significantly shifted to lower temperatures. The reduction at lower temperatures shows that the reducibility of  $\text{Co}_3\text{O}_4$  particles is easier in the case of the catalysts supported on GNS. This could be attributed to spillover of  $\text{H}_2$  from the functional groups. According to  $\text{H}_2$  spillover phenomena on GNS, where H atoms tend to group into compact clusters, possible nucleation centers can be lattice defects. In that case it lowers the reaction  $\text{H}_2$  dissociation transition state as a catalyst and reduces the nucleation barrier so the defects pre-sent on the surface of the GNS facilitate the reduction by accelerating  $\text{H}_2$  spillover [17]. Typically, the ratio of the hydrogen consumed in the first reduction step to that consumed in the second reduction step is about 1:3. The amount of hydrogen consumed in the first reduction peak was lower than the expected amount; this could only be ascribed to the reduction of nitrates rather than the reduction of  $\text{Co}_3\text{O}_4$  [18]. As shown, increasing the metal loading for the catalysts supported on GNS decreases the reduction peak temperatures and makes the catalysts reduction easier. This is due to easier reduction of larger cobalt particles on the catalysts with higher cobalt loadings and as a result larger cobalt particles [16].

The results of hydrogen TPD and oxygen titrations for all the catalysts are presented on Table 2.

Table 2. Crystallite sizes of unreduced cobalt particles determined by  $\text{H}_2$  temperatures programmed desorption and pulse reoxidation of catalysts.

Catalyst	$\mu$ mole $\text{H}_2$ desorption /g cat.	$\mu$ mole $\text{O}_2$ Consumption /g cat.	%Red.	%Dispersion	dp (nm)
C <sub>1</sub>	87	395	61.8	33.2	4.0
C <sub>2</sub>	167	874	68.3	28.93	4.6
C <sub>3</sub>	246	1382	72	21.6	6
C <sub>4</sub>	305	1952	76.3	17.55	7.5
C <sub>5</sub>	411	2530	79.1	15.05	8.7
C <sub>6</sub>	444	3036	81.7	8.95	14.5
C <sub>7</sub>	443.8	3572	82.4	7.4	17.6
A <sub>1</sub>	77	601	32.00	6.02	16.6

Comparing the results of 15wt.%  $\text{Co}/\text{GNS}$  and 15wt.%  $\text{Co}/\gamma\text{-Al}_2\text{O}_3$  catalysts, the hydrogen uptake increased by a factor of 3.2 by using GNS as cobalt catalyst support. In agreement with the results of TPR, results in this Table indicate that a remarkable improvement in the percentage reduction is obtained by switching to GNS support with the same loading (i.e. increased by a factor of 2.29). While the dispersion of the cobalt crystallites calculated based on the total amount of cobalt increased significantly, the average cobalt particle size decreased which

is due to higher surface area of GNS, lower degree of agglomeration of the cobalt crystallites and lower interaction of cobalt with support in GNS supported catalyst. These results are in agreement with the results of XRD and TEM. Larger dispersion and lower cobalt cluster size will increase greatly the number of sites available for FT reaction in GNS supported catalysts with the same loading.

This table shows that for GNS supported catalysts the hydrogen uptake increased with increasing the amount of cobalt added up to 30wt.% then leveled off. The percentage reduction shows a remarkable increase with the increase in the amount of cobalt, while the dispersion of the cobalt crystallites decreases significantly. This table shows that increasing the amount of cobalt causes a remarkable increase in cobalt particle size, which is due to the agglomeration of the cobalt crystallites with increase in the cobalt loading. The improvements in the percentage reduction with the cobalt loading for GNS supported catalysts can be attributed to the easier reduction of larger cobalt clusters [10,16,19].

### 3.2. Activity and products selectivity and catalyst stability results

The results of Fischer-Tropsch synthesis rate (g HC produced/ g cat/ h), and the percentage CO conversion at 220°C, 1.8MPa, and a H<sub>2</sub>/CO ratio of 2 for A<sub>1</sub> and C<sub>3</sub> catalysts are given in Table 3. Data on this table reveals that cobalt catalyst supported on GNS significantly enhances the CO conversion and FT synthesis rate. CO conversion and the FTS rate show an increase of about 84% in accordance with hydrogen uptake, percentage reduction and percentage dispersion (Table 2). Table 3 reveals that the FTS rate and CO conversion are strongly dependent and proportional to the number of surface reduced active cobalt sites. It is to note that the rate of water gas shift reaction or CO<sub>2</sub> formation rate was negligible for both catalysts [10].

Table 3. Activity Products selectivity of 15wt.% Co/Graphene and 15wt.% Co/ $\gamma$ -Al<sub>2</sub>O<sub>3</sub>

Catalyst	% CO Conversion	C <sub>5</sub> <sup>+</sup>	CH <sub>4</sub>	C <sub>2</sub> -C <sub>4</sub>	Rate (gr CH/gr cat./hr)
C <sub>3</sub>	73.2	78.8	13.5	7.7	0.321
A <sub>1</sub>	39.9	82.2	11.3	6.5	0.18

The change in CO conversion and FT synthesis rate could be possibly explained by perusing the structural and electronic properties of Co/GNS catalyst. It has been shown that the Co atom serves as a donor to supply electrons, which are partly transferred to saturate the electronic states of carbon atoms in the GNS and the rest transferred to bind the gas adsorption. CO molecules as acceptors gain electrons from the Co/GNS substrates. Gaining more electrons will result more stable adsorptions. However, the enhanced electron transfer from carbon atoms to the adsorbed H<sub>2</sub> is the main drive for H<sub>2</sub> dissociation and this could increase the density of reactants, and hence create a locally higher concentration which will favor CO hydrogenation [20-21]. The presence of the OH groups on GNS and the more surface reduced Co atoms, which are present on Co/GNS catalyst accelerates charge transfers [22].

Table 3 also shows the effects of support on the selectivity of Fischer-Tropsch synthesis products. Comparing the product distributions for A<sub>1</sub> and C<sub>3</sub> catalysts, clearly demonstrates that, unlike to the significant improvement in the CO conversion and FTS rate, product distribution shows a slight shift to lower molecular weight hydrocarbons in GNS supported cobalt catalyst. C<sub>5</sub><sup>+</sup> selectivity is decreased by 4.3%, CH<sub>4</sub> selectivity is increased by 16.3% and C<sub>2</sub>-C<sub>4</sub> light gaseous hydrocarbons is increased by 15.6% for GNS supported catalyst. It is believed that in FTS the larger cobalt particles are more selective to larger hydrocarbons and the smaller particles are selective for methane and light gases [19]. It seems that for A<sub>1</sub> catalyst, which has larger cobalt clusters (Table 2), the steric hindrance for dissociative adsorption of CO and -CH<sub>2</sub>- monomer and addition of this monomer to the growing chain is less. On the other hand, chain propagation and growth probability at the surface of the large clusters of A<sub>1</sub> catalyst is more than that of the smaller clusters of C<sub>3</sub> catalyst [23]. The increase in methane and light gaseous products and the decline of C<sub>5</sub><sup>+</sup> hydrocarbons for GNS supported catalyst is not significant compa-

ring to the large improvement of FTS rate of 84%. In industrial scale, increasing the methane and light gaseous products selectivity will slightly increase the amount of recycling to syngas production unit resulting in larger syngas and FT reactors and higher capital cost of the plant. However, in the case of the GNS supported cobalt catalyst 84% enhancement of reaction rate will decrease the size of FT reactor and hence the capital cost, significantly. Process optimization and overall economical calculations are necessary to determine the effects of these variables on the capital cost of an industrial plant.

Figure 4 presents the variations of FTS rate with the cobalt loadings for Co/GNS and Co/ $\gamma$ -Al<sub>2</sub>O<sub>3</sub> catalysts. It is to note that the data for Co/ $\gamma$ -Al<sub>2</sub>O<sub>3</sub> catalysts are taken out from ref. [24]. This figure shows that for Co/GNS catalysts the FTS rate increases with increasing the amount of cobalt loading reaches a maximum at the cobalt loading of 30 wt.% and then slightly decreases. However for Co/ $\gamma$ -Al<sub>2</sub>O<sub>3</sub> catalysts the maximum activity is obtained at 25wt.% cobalt loading. The loading of more cobalt on the GNS is the result of higher surface area and higher pore volume of the GNS in comparison to  $\gamma$ -Al<sub>2</sub>O<sub>3</sub>. Consequently, not only GNS supported catalysts are more active than the alumina supported catalysts with the same loading, but also the amount of maximum cobalt loading on the GNS is higher than the alumina supports.

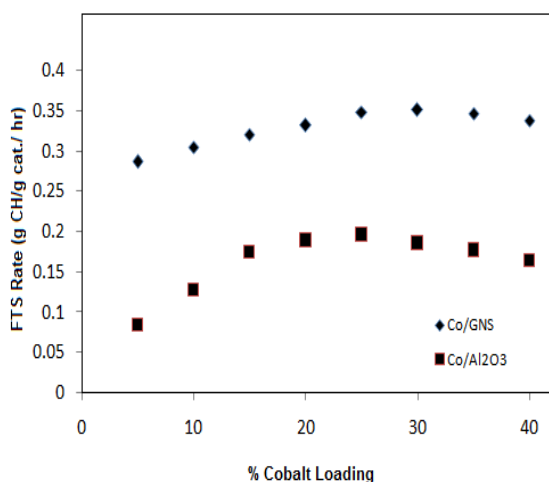


Figure 4. Variations of FTS rate with the cobalt loadings for Co/GNS and Co/ $\gamma$ -Al<sub>2</sub>O<sub>3</sub> catalysts

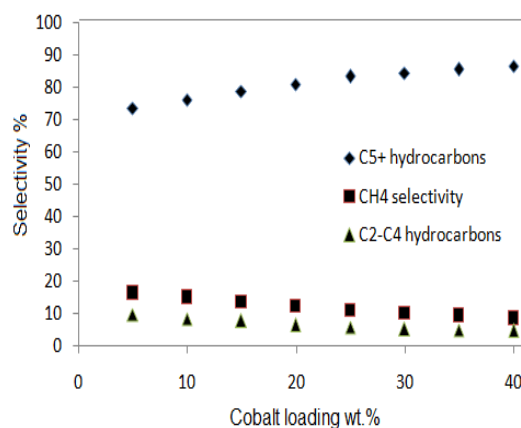


Figure 5. Variations of products selectivity for GNS supported catalysts with cobalt loading.

In industrial scale, GNS supported FT synthesis catalysts with high productivity will decrease reactor volume requirements. Since FT reaction is not a fast reaction, industrial scale FT reactors are very big reactors. Therefore, using GNS supported cobalt catalyst can decrease the industrial scale reactors volume and improve process economics significantly. On the other hand, in order to increase the reducibility and activity of the conventional  $\gamma$ -Al<sub>2</sub>O<sub>3</sub> supported cobalt catalysts, ruthenium and rhenium are used as cobalt catalyst promoters [15]. Indeed, these promoters can increase the reducibility and activity of the conventional metal oxide supported cobalt catalysts, the application of ruthenium and rhenium as cobalt catalyst promoters in FTS is restricted due to their high price. Excellent reducibility and high activity of GNS supported cobalt catalysts makes it a suitable candidate for industrial FT processes and eliminate the need for such costly promoters.

Figure 5 shows the variation of products selectivity for GNS supported cobalt catalysts. As shown, increasing the Co loading increases the C<sub>5</sub><sup>+</sup> hydrocarbons selectivity and decreases the selectivity of methane and other light gaseous hydrocarbons. Increasing the cobalt loading increases the cobalt average particle sizes (Table 2) which in turn leads to increase in the selectivity of heavy hydrocarbons.

Figure 6 shows the variations of CO conversion with the time on stream (TOS) for 15wt.% Co/GNS and 15wt.% Co/ $\gamma$ -Al<sub>2</sub>O<sub>3</sub> catalysts. As shown, for 15wt.% Co/GNS catalyst, 240 hrs continues FT synthesis decreased the % CO conversion from 78.9 to 74.8% (i.e. 5.2% decrease

in catalyst activity). At the same time for Co/ $\gamma$ -Al<sub>2</sub>O<sub>3</sub> catalyst the % CO conversion decreased from 39.9 to 32% (i.e.19.8% decrease in catalyst activity).It has been shown that water produced during the FT synthesis is the main reason for catalyst deactivation [25-26]. Recent experimental works indicate that the contact angle of water on GNS is significantly higher than that of other supports. This suggests that GNS could be one of the most hydrophobic surfaces with very weak interaction with the water molecules [27]. This will decrease the water induced oxidation of cobalt, formation of compounds between cobalt and support and the oxidation-reduction cycles on the catalyst surface which led to the sintering or cluster growth [27].

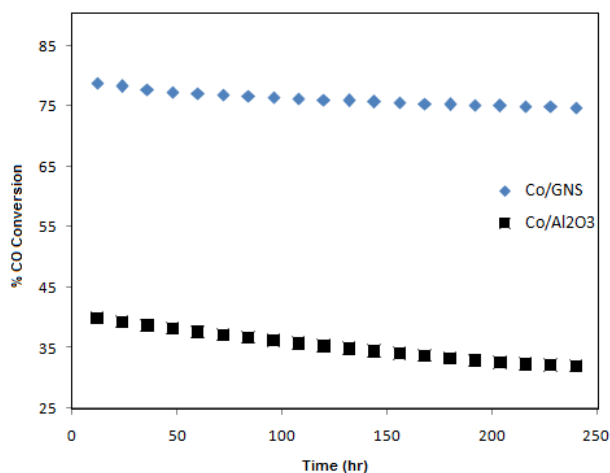


Figure 6. Variations of %CO conversion with time-on-stream for Co/GNS and Co/ $\gamma$ -Al<sub>2</sub>O<sub>3</sub> catalysts

#### 4. Conclusion

GNS was used as cobalt FTS catalyst support. Using GNS as cobalt catalyst support decreased the average cobalt particles size, increased cobalt dispersion and improved the catalyst reducibility. From a catalytic activity standpoint, the performance of catalyst in FTS considerably enhanced in comparison with that obtained from cobalt on  $\gamma$ -Al<sub>2</sub>O<sub>3</sub>. The products selectivity showed a slight shift to lower molecular weight hydrocarbons. GNS increased the catalyst stability. For Co/GNS catalysts the FTS rate increased with increasing the amount of cobalt loading reached a maximum at the cobalt loading of 30 wt.% and then slightly decreased. However for Co/ $\gamma$ -Al<sub>2</sub>O<sub>3</sub> catalysts the maximum activity is obtained at 25wt.% cobalt loading. Using GNS as catalyst support increased the catalyst lifetime.

#### References

- [1] Dry ME. The Fischer-Tropsch process: 1950–2000. *Catalysis today*. 2002; 71(3): 227-41.
- [2] Vogel AP, van Dyk B, Saib AM. GTL using efficient cobalt Fischer-Tropsch catalysts. *Catalysis Today*. 2016; 259:323-30.
- [3] Pendyala VR, Jacobs G, Bertaux C, Khalid S, Davis BH. Fischer-Tropsch synthesis: Effect of ammonia on supported cobalt catalysts. *Journal of Catalysis*. 2016; 337:80-90.
- [4] Delgado JA, Claver C, Castellón S, Curulla-Ferré D, Ordonsky VV, Godard C. Effect of polymeric stabilizers on Fischer-Tropsch synthesis catalyzed by cobalt nanoparticles supported on TiO<sub>2</sub>. *Journal of Molecular Catalysis A: Chemical*. 2016; 417: 43-52.
- [5] Arsalanfar M, Mirzaei AA, Bozorgzadeh HR, Samimi A, Ghobadi R. Effect of support and promoter on the catalytic performance and structural properties of the Fe-Co-Mn catalysts for Fischer-Tropsch synthesis. *Journal of Industrial and Engineering Chemistry*. 2014; 20(4):1313-23.

- [6] Orita H, Naito S, Tamaru K. Mechanism of formation of C<sub>2</sub>-oxygenated compounds from CO+H<sub>2</sub> reaction over SiO<sub>2</sub>-supported Rh catalysts. *Journal of Catalysis*. 1984; 90(2):183-93.
- [7] Karimi S, Tavasoli A, Mortazavi Y, Karimi A. Enhancement of cobalt catalyst stability in Fischer–Tropsch synthesis using graphene nanosheets as catalyst support. *Chemical Engineering Research and Design*. 2015; 104: 713-22.
- [8] Jacobs G, Das TK, Zhang Y, Li J, Racoillet G, Davis BH. Fischer–Tropsch synthesis: support, loading, and promoter effects on the reducibility of cobalt catalysts. *Applied Catalysis A: General*. 2002; 233(1):263-81.
- [9] Qin Z, Taylor M, Hwang M, Bertoldi K, Buehler MJ. Effect of wrinkles on the surface area of graphene: toward the design of nanoelectronics. *Nanoletters*. 2014; 14(11): 6520-5.
- [10] Tavasoli A, Sadaghiani K, Nakhaeipour A, GhalbiAhangari M. Cobalt Loading Effects on the Structure and Activity for Fischer-Tropsch and Water–gas Shift Reactions of Co/Al<sub>2</sub>O<sub>3</sub> Catalysts. *Iran. J. Chem. Chem. Eng. Vol.* 2007; 26(1).
- [11] Tavasoli AH, Sadaghiani K, Khorashe F, Seifkordi AA, Rohani AA, Nakhaeipour A. Cobalt supported on carbon nanotubes—a promising novel Fischer–Tropsch synthesis catalyst. *Fuel Processing Technology*. 2008; 89(5):491-8.
- [12] Tavasoli A, Abbaslou RM, Trepanier M, Dalai AK. Fischer–Tropsch synthesis over cobalt catalyst supported on carbon nanotubes in a slurry reactor. *Applied Catalysis A: General*. 2008; 345(2):134-42.
- [13] Davis BH, Iglesia E. Technology development for iron and cobalt Fischer-Tropsch catalysts final technical report. Contract No. DE-FC26-98FT40308 [R/OL]. <http://www.fischei^tropsch.Org/DOE/DOE-REPORT>. 2002; 3.
- [14] Sun S, Wang C, Chen M, Zheng J. A novel method to control atomic defects in graphene sheets, by selective surface reactions. *Applied Surface Science*. 2013; 283: 566-70.
- [15] Jermwongratanachai T, Jacobs G, Shafer WD, Pendyala VR, Ma W, Gnanamani MK, Hopps S, Thomas GA, Kitiyanan B, Khalid S, Davis BH. Fischer–Tropsch synthesis: TPR and XANES analysis of the impact of simulated regeneration cycles on the reducibility of Co/alumina catalysts with different promoters (Pt, Ru, Re, Ag, Au, Rh, Ir). *Catalysis Today*. 2014; 228: 15-21.
- [16] Potoczna-Petru D, Kępiński L. Reduction study of Co<sub>3</sub>O<sub>4</sub> model catalyst by electron microscopy. *Catalysis letters*. 2001; 73(1):41-6.
- [17] Lin Y, Ding F, Yakobson BI. Hydrogen storage by spillover on graphene as a phase nucleation process. *Physical Review B*. 2008; 78(4):041402.
- [18] Trépanier M, Tavasoli A, Anahid S. Deactivation Behavior of Carbon Nanotubes Supported Cobalt Catalysts in Fischer-Tropsch Synthesis. *Iran. J. Chem. Chem. Eng.* 2011; 30(1): 37-47.
- [19] Yang J, Frøseth V, Chen D, Holmen A. Particle size effect for cobalt Fischer–Tropsch catalysts based on in situ CO chemisorption. *Surface Science*. 2015 Oct 24.
- [20] Reuel RC, Bartholomew CH. Effects of support and dispersion on the CO hydrogenation activity/selectivity properties of cobalt. *Journal of Catalysis*. 1984; 85(1): 78-88.
- [21] Gallouze M, Kellou A, Drir M. Electronic and magnetic properties of adsorbed H<sub>2</sub> on graphene with atomic defects: Ab initio study. *Physica E: Low-dimensional Systems and Nanostructures*. 2013; 52: 127-35.
- [22] Wang N, Wang L, Tan Q, Pan YX. Effects of hydroxyl group on H<sub>2</sub> dissociation on graphene: A density functional theory study. *Journal of Energy Chemistry*. 2013; 22(3): 493-7.
- [23] Chen J, Liu ZP. Origin of selectivity switch in Fischer–Tropsch synthesis over Ru and Rh from first-principles statistical mechanics studies. *Journal of the American Chemical Society*. 2008; 130(25): 7929-37.

- [24] Tavasoli A., Catalyst composition and its distribution effects on the enhancement of activity, selectivity and suppression of deactivation rate of FTS cobalt catalysts. Ph.D. Thesis, University of Tehran, 2005.
- [25] Hou C, Xia G, Sun X, Wu Y, Jin C, Yan Z, Li M, Hu Z, Nie H, Li D. Thermodynamics of oxidation of an alumina-supported cobalt catalyst by water in FT synthesis. *Catalysis Today*.2015; 264: 91-97.
- [26] Tsakoumis NE, Rønning M, Borg Ø, Rytter E, Holmen A. Deactivation of cobalt based Fischer–Tropsch catalysts: a review. *Catalysis Today*. 2010; 154(3): 162-82.
- [27] Soldano GJ, Juarez MF, Teo BW, Santos E. Structure and stability of graphene edges in O<sub>2</sub> and H<sub>2</sub> environments from ab initio thermodynamics. *Carbon*. 2014; 78:181-9.

---

*\*Corresponding author: Ahmad Tavassoli <tavassolia@khayam.ut.ac.ir>*